TOWARDS DEMONSTRATION OF QUANTUM BACKFLOW

WANG YIRAN

XIAMEN UNIVERSITY MALAYSIA

2024

XIAMEN UNIVERSITY MALAYSIA

厦門大學馬來西亞分校

FINAL YEAR PROJECT REPORT

TOWARDS DEMONSTRATION OF QUANTUM BACKFLOW

NAME OF STUDENT	:	WANG YIRAN
STUDENT ID	:	PHY2009484
SCHOOL/FACULTY	:	SCHOOL OF MATHEMATICS AND PHYSICS
PROGRAMME	:	BACHELOR OF SCIENCE IN PHYSICS
INTAKE	:	2020/09
SUPERVISOR	:	PROF. TOMASZ PATEREK

JUNE 2024

DECLARATION

I hereby declare that this thesis is based on my original work except for citations and quotations which have been duly acknowledged. I also declare that it has not been previously and concurrently submitted for any other degree or award at Xiamen University Malaysia or other institutions.

Signature : 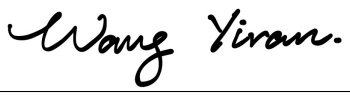

Name : Wang Yiran

ID No. : PHY2009484

Date : July 2, 2024

APPROVAL FOR SUBMISSION

I certify that this project/thesis, entitled “TOWARDS DEMONSTRATION OF QUANTUM BACKFLOW", and prepared by WANG YIRAN, has met the required standard for submission in partial fulfillment of the requirements for the award of Bachelor of PHYSICS at Xiamen University Malaysia.

Approved by,

Signature : 

Supervisor : Prof. Tomasz Paterek

Date : July 2, 2024

ACKNOWLEDGEMENTS

I would like to thank all who have contributed to this thesis throughout its development. I would like to express my gratitude to my final year project supervisor, Prof. Tomasz Paterek, his invaluable guidance, inspiration and enormous patience through out the project is indispensable to the completion of the thesis. I would also like to express my gratitude to my research co-supervisor, Prof. Arseni Goussev for his numerous support and guidance through my research. I would like to thank Dr. Lim Yen Kheng for his inspiration on some of the issues I have encountered throughout the project.

ABSTRACT

Quantum backflow describes a phenomenon where arguably forward propagating particle locally propagates backwards. Experiments have only demonstrated backflow using strong beams in the optics domain and observation of backflow with truly quantum objects, say individual photons or electrons, is still missing. Here, we systematically review the concepts which lead to quantum backflow and provide a simple example of backflowing wave function which to a large extend can be treated analytically and is experimentally implementable.

Keywords: quantum backflow, superoscillation, suboscillation, plain momentum distribution

CONTENTS

1 Introduction and Literature Review **1**

2 What is Quantum Backflow **2**

2.1 Global and local momentum 2

2.2 Superoscillations and Suboscillations 5

2.3 Quantum backflow as suboscillation or superoscillation 10

2.4 Quantum backflow in terms of probability current 11

2.5 Quantum backflow in terms of spatial probability 14

3 Experimentally Accessible Example **16**

3.1 Numerical Evidence of Backflow in Single Slit Experiment 17

3.2 Analytical Derivation 19

4 Discussion on the Example **26**

5 Conclusion **28**

LIST OF FIGURES

2.1 A typical behaviour of global and local momenta. 4
2.2 Probability Distribution and Global Momentum of Wave Function given above. 5
2.3 Superoscillations and suboscillations. 6
2.4 Superoscillations and suboscillations for the normalised wave function in Eq. (2.12). 8
2.5 Suboscillations in optical beams. 9
2.6 Quantum backflow as suboscillation. 11
2.7 Oscillating probability flux and local momentum. 15

3.1 Evolution of probability distribution. 17
3.2 Spacial distribution of backflow. 18
3.3 Change of upper and lower limit of the integral. 20
3.4 Inversely oriented curve of the integral. 24
3.5 Analytical approach to backflow. 25

4.1 Backflow analysis on spacial distribution and time-evolution. 27

LIST OF SYMBOLS

A	:	constant defined by example accordingly
a	:	constant defined by example accordingly
B	:	constant defined by example accordingly
b	:	constant defined by example accordingly
e	:	natural constant, or Euler number
$\hbar$	:	reduced Planck constant
i	:	imaginary unit
J	:	Jacobian determinant
$J_0(x)$	:	one of Bessel functions of the first kind
$j(x)$	:	probability flux
k	:	wave number
k_l, k_{local}	:	local wavenumber (local momentum)
m	:	mass of the particle
∇	:	nabla symbol as gradient operator
P	:	possibility
p	:	momentum
p_0	:	center of momentum distribution
ψ	:	a general notation of wave function
t	:	time
u	:	variable used in change of variable method
v	:	variable used in change of variable method
w	:	width of flat momentum distribution
x	:	spacial measurement in position space

CHAPTER 1

INTRODUCTION AND LITERATURE REVIEW

Propagation of waves has remarkable and often counter-intuitive features. The usual examples of diffraction or interference have recently been augmented with the case of backflow. In backflow, a wave that has only negative momenta (and hence moves towards negative direction) can still display locally signs of motion in positive direction. These signs could be in the form of local momentum, local current or intensity increment. This effect has been observed with optical beams [Eliezer et al., 2020, Daniel et al., 2022, Ghosh et al., 2023] and can be seen as a special case of a broader class of phenomena called superoscillations and suboscillations [Chen et al., 2019].

Originally, the idea of quantum backflow appeared in the literature on quantum mechanics [Allcock, 1969, Kijowski, 1974, Bracken and Melloy, 1994], which is also a form of wave theory but for individual quanta. Yet, quantum backflow, i.e. backflow of individual quantum particles, has not yet been demonstrated. This is the main motivation behind the present thesis. We will now gradually introduce all the concepts related to quantum backflow that culminate in three, at first sight different, definitions of the phenomenon. We will argue that some of them are actually equivalent. Various examples will be presented that illustrate certain important points, and we will stress when they are calculated here for the first time. Finally, we will provide a simple example of backflowing wave function that is suited for experimental demonstration.

The example is based on the flat momentum distribution and could be realised with a help of a single slit and some specific lens setup realising the Fourier transformation in optical experiments [Wilson and McCreary, 1995]. The time evolution of such flat momentum distribution will end up with a dynamical backflow defined accordingly. It is a bit surprising that such a simple example has been overlooked in the literature. We believe that this is because many works have focused on mathematical aspects of backflow, which seem optimised for non-normalisable wave packets [Penz et al., 2005].

CHAPTER 2

WHAT IS QUANTUM BACKFLOW

2.1 Global and local momentum

In quantum mechanics as well as other wave theories one can distinguish between local and global properties. Momentum is a prime example of a global property. In order to determine it, one needs to determine the wavelength which can only be done if a considerable part of the wave function is accessible. In contradistinction the probability to find a particle near a given point or a probability current are well known local properties because they can be determined given just a small part of the wave function. A less well known local quantity of high interest in this report is so-called "local momentum" to be defined below.

In order to introduce the local momentum formally let us first recall the usual treatment of momentum in quantum mechanics. Consider a simple situation, where a particle is moving in one dimension, say along x axis. In position representation the momentum operator is given by

$$\hat{p} = -i\hbar\frac{\partial}{\partial x}, \tag{2.1}$$

and it acts on the whole wave function and produces another wave function defined on the whole of the x axis. The eigenstates of the global momentum operator are plane waves $\exp(ikx)$, where $p = \hbar k$, and correspondingly in order to determine possible outcomes of the momentum measurement (momentum spectrum) one needs to perform the Fourier transform of the wave function $\psi(x)$ describing the system:

$$\tilde{\psi}(k) = \frac{1}{\sqrt{2\pi}}\int_{-\infty}^{\infty}\psi(x)\,e^{-ikx}dx. \tag{2.2}$$

Again this emphasises the global character of momentum measurement where the total wave function is necessary to determine the Fourier transform.

The global momentum has to be distinguished from the local momentum, whose values

are defined as follows (note that formally this is the local wave number, but the whole community calls this quantity a local momentum):

$$k_l(x_0) = \mathrm{Im}\frac{\partial}{\partial x}\left[\log\psi(x)\right]_{x_0}. \tag{2.3}$$

Here the derivative of the wave function is taken at a point x_0 and hence only this local part of $\psi(x)$ contributes to the local momentum value. The logarithm and imaginary part are chosen such that the final result returns the value in the exponent of the wave function. For example, for the plane wave $\exp(ikx)$ the local momentum is independent of x_0 and equal to k, the value of the global momentum, justifying the definition of local momentum. In three dimensions the local momentum is defined as [Berry, 2013a]:

$$\mathbf{k}_l(\mathbf{r}_0) = \nabla\mathrm{Im}[\log\psi(\mathbf{r})]|_{\mathbf{r}_0}, \tag{2.4}$$

and we denote its magnitude as $|\mathbf{k}_l(\mathbf{r})| = k_l$. It will always be clear from the context whether we discuss one or more dimensions. Local momentum is an important ingredient in calculating the orbital angular momentum of optical fields [Allen and Padgett, 2011], and forces on small particles in the field. It is therefore not a purely mathematical concept.

Example 1. To illustrate both concepts of momentum, and their usual behaviour, consider Gaussian wave packet:

$$\psi(x) = A\, e^{-\frac{x^2}{4\sigma^2}}\, e^{ik_0x},$$

where the normalization constant is $A = (2\pi)^{-1/4}\sigma^{-1/2}$. To obtain the global momentum of the wave packet, we apply the Fourier transform following Eqn. (2.2):

$$\tilde{\psi}(k) = A\sqrt{2}\sigma e^{-(k-k_0)^2\sigma^2}. \tag{2.5}$$

As seen the momentum wave function is also Gaussian, but centered at k_0. Hence the momentum spectrum is continuous with most probable values within one standard deviation from k_0. The local momentum follows from Eq. (2.3), it is independent of position and

given by

$$k_l(x_0) = k_0. \tag{2.6}$$

This is a clear example of how the local momentum is different from the global momentum. But the final outcome might be anticipated because the local momentum is just the most probable momentum in the spectrum. Fig. 2.1 provides the illustration.

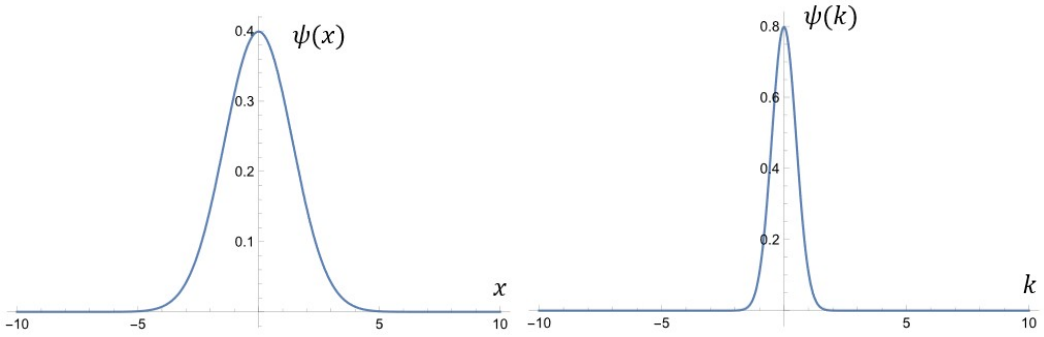

(a) Wave function $\psi(x)$ (b) Global momentum $\tilde{\psi}(k)$

Figure 2.1: A typical behaviour of global and local momenta.
(a) Gaussian wave function (b) Momentum wave function for the case $k_0 = 0$. In this case, the local momentum is just the most probable global momentum, i.e. $k_l(x_0) = k_0 = 0$, independently of x_0.

Example 2. In the following example we choose the global momentum within a finite range and with a constant probability density. As expected the local momentum is between the minimum and maximum of the global momentum. The position wave function reads:

$$\psi(x) = \frac{1}{\sqrt{\pi}} \frac{\sin x}{x}. \tag{2.7}$$

Applying the Fourier transformation of Eqn. (2.2) gives the "barrier" function:

$$\tilde{\psi}(k) = \begin{cases} 1/\sqrt{2} & \text{for} \quad k \in [-1, 1] \\ 0 & \text{elsewhere} \end{cases} \tag{2.8}$$

Since the wave function is real, the local momentum is independent of x_0 and everywhere equal to zero. This situation is depicted in Fig. 2.2.

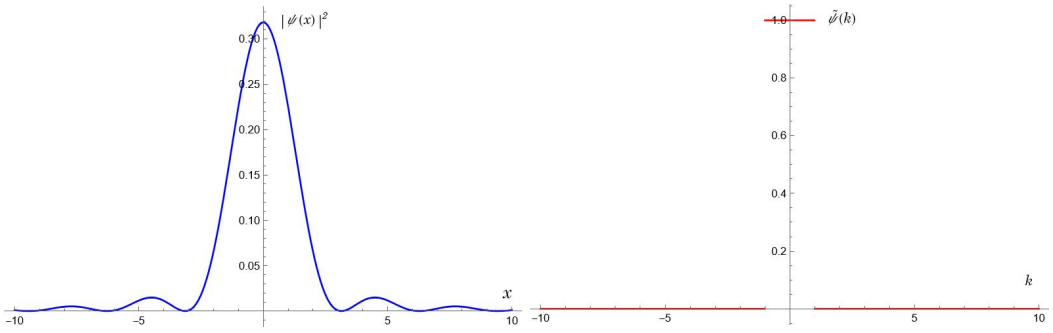

(a) Probability Distribution $\psi^2(x)$ (b) Global Momentum as $\tilde{\psi}(k)$

Figure 2.2: Probability Distribution and Global Momentum of Wave Function given above. The local momentum of the wave packet sit at $k_l(x_0) = k_0 = 0$.

The concept of local momentum, instead of a purely mathematical approach to the wave function, is a wide scale interpretation to the local properties of scalar wave [Berry, 2013a]: This concept plays a central part in the guiding equation of de Broglie-Bohm theory as the velocity of individual particles [Holland, 1995], as well as in the Madelung equations of quantum hydrodynamics [Madelung, 1927]. Furthermore, in optical diffraction, k_l could be regarded as the definition of the direction of optical particles (which later determined as photon) in the term of scalar waves.

2.2 Superoscillations and Suboscillations

The examples just given showed a typical behaviour of global and local momentum. Here we review more exotic cases that culminate in quantum backflow. We start with so-called superoscillations and suboscillations. Superoscillations happen when there exists a local momentum which is larger than the largest momentum in the Fourier spectrum. Analogically, suboscillations require local momentum to be smaller than the minimal global momentum. The mathematical general form of such oscillation, or superoscillatory function was first given by [Aharonov et al., 2011].

Example 3. Consider first the wave function given in [Eliezer and Bahabad, 2017]:

$$\psi(x) = (\cos(x) + ia\sin(x))^N, \tag{2.9}$$

where a is real and $N \in \mathbb{N}^+$. For simplicity we set $N = 1$, and rewrite the wave function using plane waves:

$$\psi(x) = \frac{a+1}{2} e^{ix} - \frac{a-1}{2} e^{-ix} = c_0 e^{ix} + c_1 e^{-ix}, \tag{2.10}$$

where c_0 and c_1 are constants determined by the value of a. Accordingly, the Fourier spectrum is composed of only two momenta, equal to ± 1. The definition of local momentum applied to the wave function (2.10) gives:

$$k_l(x) = \mathrm{Im} \frac{d}{dx} \log[f(x)] = \frac{a}{\cos^2(x) + a^2 \sin^2(x)} \tag{2.11}$$

By tuning parameter a we can obtain both superoscillations and suboscillations. Fig. 2.3 demonstrates both effects. The solid lines represent local momenta with the upper curve calculated for $a = 1.5$ and the lower curve calculated for $a = -1.5$. As seen, the local momentum periodically exceeds the maximum of global momentum (for $a = 1.5$) and minimum of global momentum (for $a = -1.5$). The plot is prepared for $a = \pm 1.5$, but the effects are present for all $|a| > 1$.

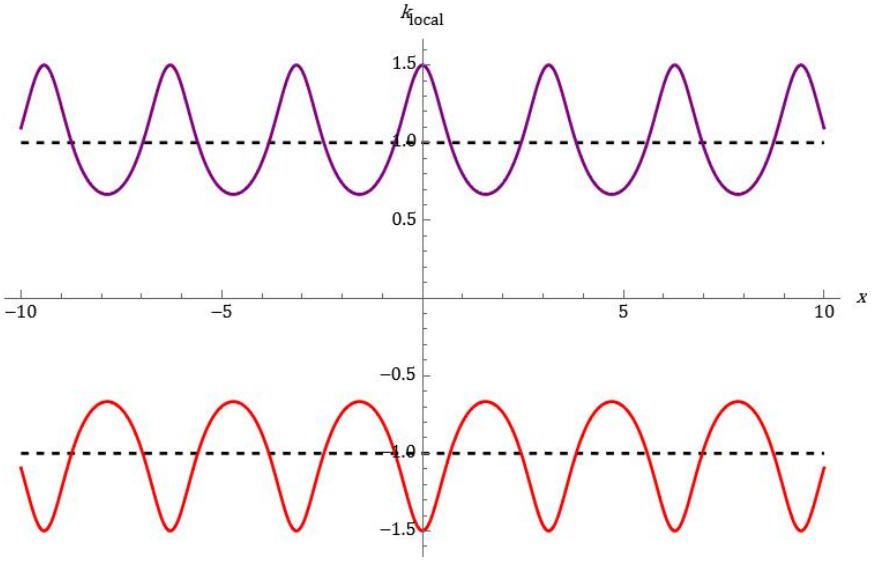

Figure 2.3: Superoscillations and suboscillations.
The dashed lines give maximum and minimum of global momenta. The solid curves show the local momentum. The top curve is calculated for $a = 1.5$ and since the local momentum exceeds maximal global momentum it is an example of superoscillations. The bottom curve is for $a = -1.5$ and since local momentum is below the minimal global momentum we deal with suboscillations.

Example 4. One may complain that in the Example 3 the wave function is not normalisable for all values of a, and accordingly perhaps there is no physical system where superoscillations and suboscillations can actually be observed. It would therefore be desirable to produce normalised wave functions exhibiting these effects. The first new result of this thesis is the following normalised example:

$$\psi(x) = \sqrt{\frac{1}{\pi(a^2+1)}} J_0(x)(\cos x + ia \sin x), \tag{2.12}$$

where $J_0(x) = \sin(x)/x$ is one of the Bessel functions of the first kind. This wave function is band-limited as well as superoscillating. To show this we take the Fourier transformation:

$$\tilde{\psi}(k) = \frac{1}{\sqrt{2\pi}} \int_{-\infty}^{\infty} dx \sqrt{\frac{1}{\pi(a^2+1)}} \frac{\sin x}{x} (\cos x + ia \sin x) e^{-ikx}. \tag{2.13}$$

Using Eq. (2.10) for the expression in the bracket, the integral becomes proportional to

$$\begin{aligned} \tilde{\psi}(k) &\sim \int_{-\infty}^{\infty} dx \frac{\sin x}{x} (\cos x + ia \sin x) e^{-ikx} \\ &= \frac{a+1}{2} \int_{-\infty}^{\infty} dx \frac{\sin x}{x} e^{-i(k-1)x} - \frac{a-1}{2} \int_{-\infty}^{\infty} dx \frac{\sin x}{x} e^{-i(k+1)x}. \end{aligned} \tag{2.14}$$

Since the range of $\frac{\sin x}{x}$ in k space is $-1 < k < 1$, and the flat momentum distribution of $\frac{\sin x}{x} e^{-ik_0 x}$ is centered at k_0, we conclude that $\tilde{\psi}(k)$ in Eq. (2.14) has spectrum which is the sum of the range $0 < k < 2$ and the range $-2 < k < 0$. This is clearly a band-limited global momentum. At the same time the local momentum of the wave function is given by:

$$k_l(x) = \mathrm{Im} \frac{\partial}{\partial x} \log[\psi(x)] = \frac{1}{\sqrt{\pi(a^2+1)}} \left[\frac{\sin 2x}{\sin^2 x} - \frac{1}{x} \right]. \tag{2.15}$$

Both local and global momenta are plotted in Fig. 2.4, which shows clear evidence for both superoscillations and suboscillations.

Experimental observations of superoscillations and suboscillations were given in various experimental schemes. Some experiments aimed at measuring the one-dimensional transverse local momentum of super-oscillatory optical beam by applying slit-scanning proce-

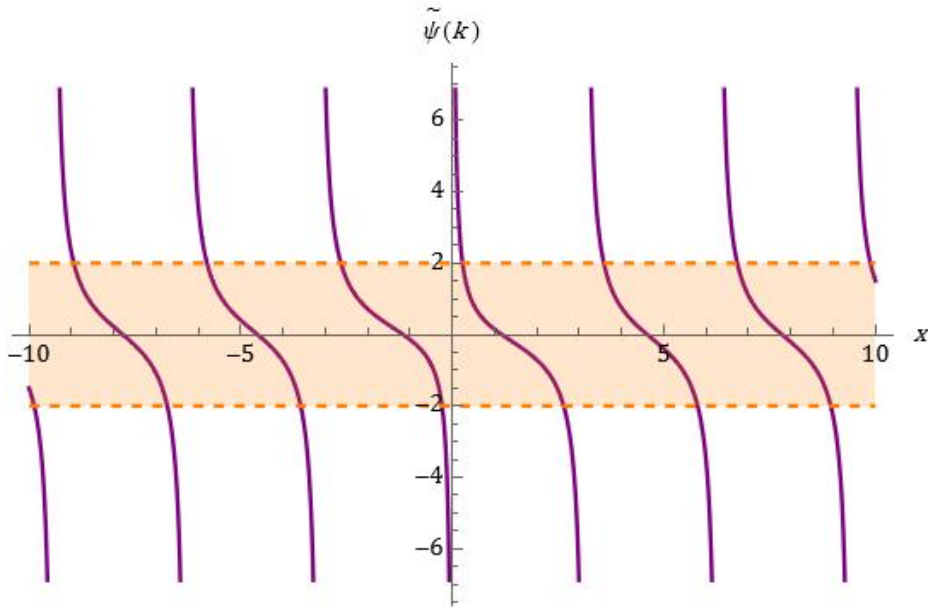

Figure 2.4: Superoscillations and suboscillations for the normalised wave function in Eq. (2.12).
The violet curves present the local momentum and the yellow range of $[-2, 2]$ excluding 0 is the range of global momenta. Here $a = -1.5$.

dure [Eliezer et al., 2020] or Shack-Hartmann wavefront sensor [Daniel et al., 2022]. In these works the teams have measured local momentum and we would like to illustrate the suboscillation explicitly using their wave function.

Consider the superposition of two plane waves with unequal amplitudes, but equally inclined to the z-axis:

$$\psi(x, z) = e^{i(z+ax)} + b\, e^{i(z-ax)}, \tag{2.16}$$

where b is the ratio between two amplitudes, a is the measure of the angle between the propagation directions of the two plane waves [the angle is given by $2\arctan(a)$], and x is one of the transverse directions. To find the global momentum in the transverse direction we take the Fourier transform with respect to x, which up to a global phase e^{iz}, equals

$$\tilde{\psi}(k) = \sqrt{2\pi}[\delta(k-a) + b\,\delta(k+a)]. \tag{2.17}$$

Therefore, along x axis, the particle either moves to the right or to the left with momentum

a. The local momentum of the superposed plane waves is given by:

$$k_{local} = \frac{a - ab^2}{1 + b^2 + 2b\cos 2ax}. \tag{2.18}$$

Fig. 2.5 shows the local momentum at various points in space and marks the suboscillatory regions.

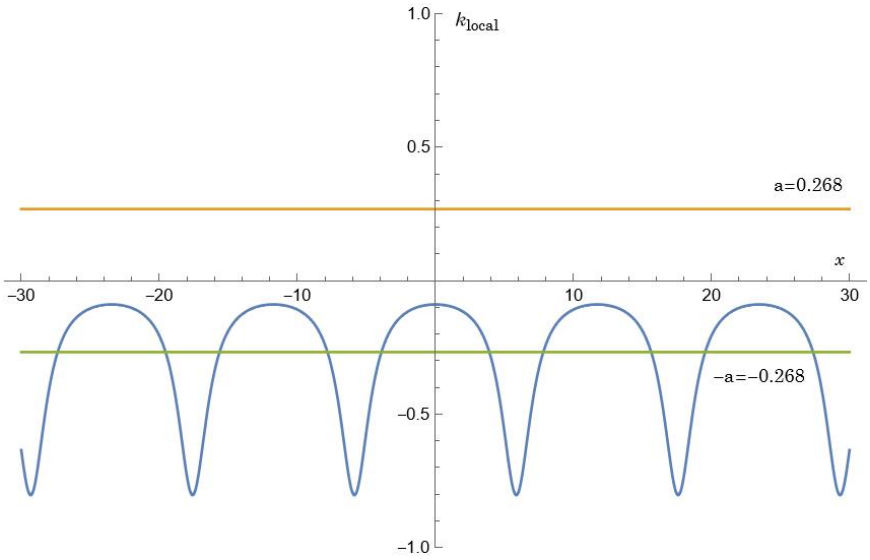

Figure 2.5: Suboscillations in optical beams.
The blue curve shows the local momentum of the wave function in Eq. (2.16) with parameters $a = 0.268$ and $b = 2$. The green line shows the lowest global momentum.

Numerous practical examples were realised to verify the superoscillation or suboscillation effect. Meta-surface interferometer experiment by [Yuan et al., 2017] measured the phase of the superoscillatory field. The superoscillatory field was formed by focusing two beams of lights after specially patterned surface.

While the presence of superoscillation in classical optics, that can be produced by periodical diffraction grating in propagating beams, was predicted by [Berry and Popescu, 2006], experimental observations of the phenomenon, specifically the optical superoscillations, were realised only recently [Zheludev and Yuan, 2022]: one of the methods used is the superoscillatory lens (SOL). In the practical design of SOLs, the local super-oscillation regions in the spectrum are generally referred to as "hotspots" and enable superoscillatory imaging with resolution beyond the Rayleight limit. A fashionable design these days is to

apply the negative index metamaterials to achieve the complete freedom in designing, by manipulating the transmissivity and retardation freely in every part of SOL. This concept, namely superoscillatory metamaterial lens (SML), however, remains a conceptual design.

In a wider scope, superoscillation (and suboscillation) are very common phenomena in reality [Rogers and Zheludev, 2013, Dennis et al., 2008], especially in optical random systems. In a two-dimensional speckle pattern, one third of area on average is super-oscillatory. Furthermore, in one-dimensional cases the local momentum can be several times larger than the maximum momentum of input waves. Other practical examples, namely Bessel beams [Berry, 2013b], are also found to perform superoscillation in certain circumstances.

2.3 Quantum backflow as suboscillation or superoscillation

Quantum backflow is a form of suboscillation where the global momenta are all non-negative and yet there are points where the local momentum is negative. So based on global momentum we would argue that the particle is moving, say, to the right, but there are regions where it flows backwards, hence the name. Of course similarly one could think of the global momentum being negative and local momentum positive. Given the previous section, we propose the simplest example of quantum backflow as the following (unnormalised) wave function:

$$\psi(x) = (\cos(x) + ia\sin(x))\, e^{ix} = \frac{a+1}{2} e^{i2x} - \frac{a-1}{2}. \tag{2.19}$$

We have effectively shifted the global momentum from $\{-1, 1\}$ to $\{0, 2\}$. The local momentum reads:

$$k_l(x) = \frac{a}{\cos^2(x) + a^2 \sin^2(x)} + 1. \tag{2.20}$$

Fig. 2.6 shows that the local momentum is negative at suitable points in space.

A similar type of backflow has recently been experimentally observed with classical optical beams having positive local orbital momentum while carrying only negative global angular momenta [Ghosh et al., 2023].

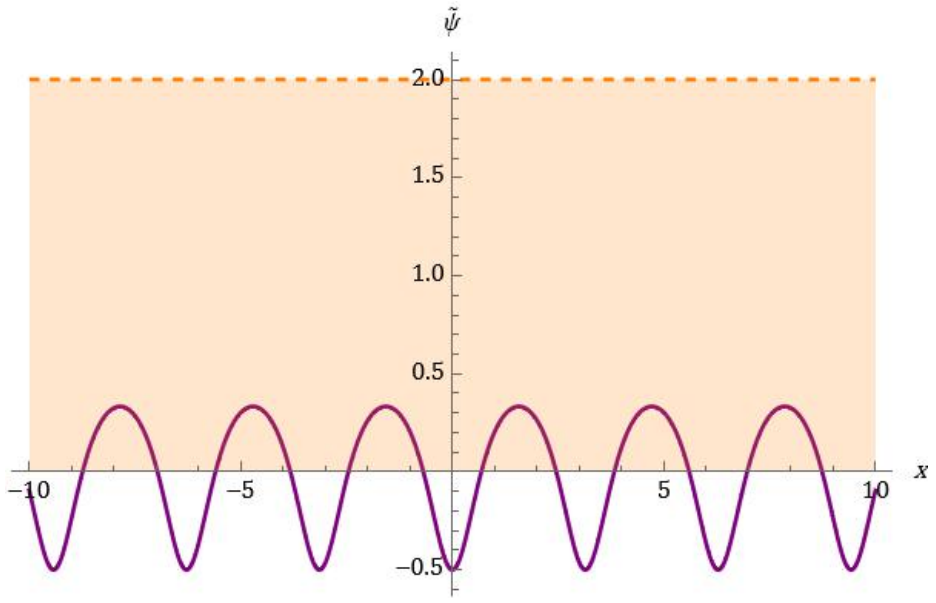

Figure 2.6: Quantum backflow as suboscillation.
Shaded area indicates the range in between the global spectrum $\{0, 2\}$. The local momentum is plotted in solid line and is computed for $a = -1.5$. It becames periodically negative, showing that despite global motion to the right, the particle flows to the left locally.

2.4 Quantum backflow in terms of probability current

An alternative approach to quantum backflow does not involve local momentum, but a closely related concept of the probability current. Recall that the probability current is given by:

$$j(x_0) = \frac{\hbar}{m} \mathrm{Im}\left(\psi^*(x_0)\frac{\partial}{\partial x}\psi|_{x_0}\right). \tag{2.21}$$

In these terms, quantum backflow occurs when the particle has non-negative global momentum (as before) but there are points in space where the probability current is negative.

At first sight this definition looks distinct from the one using local momentum, e.g. the logarithm is not present in $j(x)$. Yet, we now demonstrate that the positions where backflow takes place, determined by these two definitions, are exactly same, i.e. we prove that $j(x_0) < 0$ if and only if $k_l(x_0) < 0$. Let us call the argument of the local momentum function as z, an arbitrary complex number:

$$\frac{\partial}{\partial x}\log[\psi(x)] = z \tag{2.22}$$

In this way the condition for negativity of the local momentum is simply $\mathrm{Im}(z) < 0$. The wave function can be written as

$$\psi(x) = e^{z\,x+C}, \tag{2.23}$$

where C is a real constant and x a real variable. We substitute this expression into the definition of j:

$$\begin{aligned} \psi^*(x)\frac{\partial\psi}{\partial x} &= e^{z^*\,x+C}\,z\,e^{z\,x+C} \\ &= z\,e^{(z+z^*)x+2C}. \end{aligned} \tag{2.24}$$

Since the argument of the exponential function is real, the imaginary part of this expression is $\mathrm{Im}(z)$. Therefore the conditions for negative local momentum and negative probability current are identical. Furthermore, we could expand the relation between the two definitions into a more general one. Assume the wave function takes an arbitrary complex form $\psi = a + ib$, then the local momentum k_{local} and probability flux $j(x)$ are given respectively:

$$\begin{aligned} k_{local} &= \mathrm{Im}\frac{\partial}{\partial x}[\log(a+ib)] \\ &= \frac{1}{a^2+b^2}\left(a\frac{\partial b}{\partial x} - b\frac{\partial a}{\partial x}\right); \end{aligned} \tag{2.25}$$

$$\begin{aligned} j(x) &= \frac{\hbar}{m}\mathrm{Im}\left[\psi^*\frac{\partial\psi}{\partial x}|_{x_0}\right] \\ &= \frac{\hbar}{m}\left(a\frac{\partial b}{\partial x} - b\frac{\partial a}{\partial x}\right). \end{aligned} \tag{2.26}$$

Therefore:

$$\frac{m}{\hbar}j(x) = |\psi|^2 k_{local}. \tag{2.27}$$

We could further generalise this relation to 3-dimensional space, where $\psi(x, y, z)$ is written in the usual Cartesian coordinates. The definition of the local momentum and probability

flux are generalized respectively:

$$\boldsymbol{k}_{local} = \nabla \mathrm{Im}[\log(\psi(x,y,z))]; \tag{2.28}$$

$$\boldsymbol{j} = \frac{\hbar}{m}\mathrm{Im}[\psi^* \nabla \psi]. \tag{2.29}$$

By repeating above argument for each Cartesian component of local momentum and probability current we find:

$$\boldsymbol{k}_{local} = \frac{1}{|\psi|^2}\frac{m}{\hbar}\boldsymbol{j}. \tag{2.30}$$

Let us now give concrete examples of backflow using the calculation of probability current. We will first present a mathematical (unnormalisable) example and then a well-behaved example. We will also illustrate with these examples the equivalence between the two backflow definitions that has just been obtained.

Example 5. For the mathematical example we follow one of the first cases of backflow, given by Bracken and Melloy [Bracken and Melloy, 1994]. Consider two superposed plane waves:

$$\psi(x, t=0) = Ae^{ik_1 x} + Be^{ik_2 x}, \tag{2.31}$$

which evolve freely, i.e. under Hamiltonian $H = \hbar^2 k^2/2m$. This gives the wave function at time t equal to:

$$\begin{aligned} \psi(x,t) &= Ae^{i\theta_1(x,t)} + Be^{i\theta_2(x,t)}, \\ \theta_n(x,t) &= k_n\, x - t\,\frac{\hbar^2 k_n^2}{2m}, \end{aligned} \tag{2.32}$$

where $n = 1, 2$. Here, A, B, k_1 and k_2 are positive constants. Clearly, the global momentum in this example has only two positive values k_1 and k_2, which are conseved at all times because the evolution is free. So arguably the particle moves in one direction only, say to the right. Yet, the probability current of the superposistion in Eq. (2.32) admits

$$j(x,t) = \frac{\hbar}{m}\left[k_1 A^2 + k_2 B^2 + (k_1 + k_2)AB\cos[\theta_1(x,t) - \theta_2(x,t)]\right]. \tag{2.33}$$

The minimum of this probability current reads $\hbar(k_1 A - k_2 B)(A - B)/m$, and it is negative when $A > B$ and $k_1 A < k_2 B$, or $A < B$ and $k_1 A > k_2 B$.

Example 6. Again, one can complain about the lack of normalisation in the above example, and therefore here we show an example with properly normalised wave functions. Let us begin with modified wave function from Eq. (2.12):

$$\psi(x) = C J_0(x)(\cos x + ia \sin x) e^{i2x}, \tag{2.34}$$

with C given in Eq. (2.12). The Fourier transform is given by:

$$\tilde{\psi}(k) = \frac{a+1}{2} \int_{-\infty}^{\infty} dx\, C \frac{\sin x}{x} e^{-i(k-3)x} - \frac{a-1}{2} \int_{-\infty}^{\infty} dx\, C \frac{\sin x}{x} e^{-i(k-1)x}, \tag{2.35}$$

and shows that the range of the global momentum is $k \in (0, 2) \cup (2, 4)$, i.e. all positive. The probability current is now given by

$$j(x) = C^2 \left(\frac{\sin x}{x} \right)^2 \sin(2x)(a+1)(a-1). \tag{2.36}$$

Fig. 2.7 shows the probability flux for $a = -1.5$ with clearly seen negative values. We also plot there local momentum to indicate that both functions are negative in exactly the same range of x. The formula for local momentum reads:

$$k_l(x) = \frac{2a^2 + a + (a+2)\cot^2 x}{a^2 + \cot^2 x} \tag{2.37}$$

2.5 Quantum backflow in terms of spatial probability

Yet another way to define quantum backflow is to require that the probability of observing the particle to the left of a reference point increases despite the fact that global momenta are all non-negative. This definition is distinct from all discussed above as for the first time one

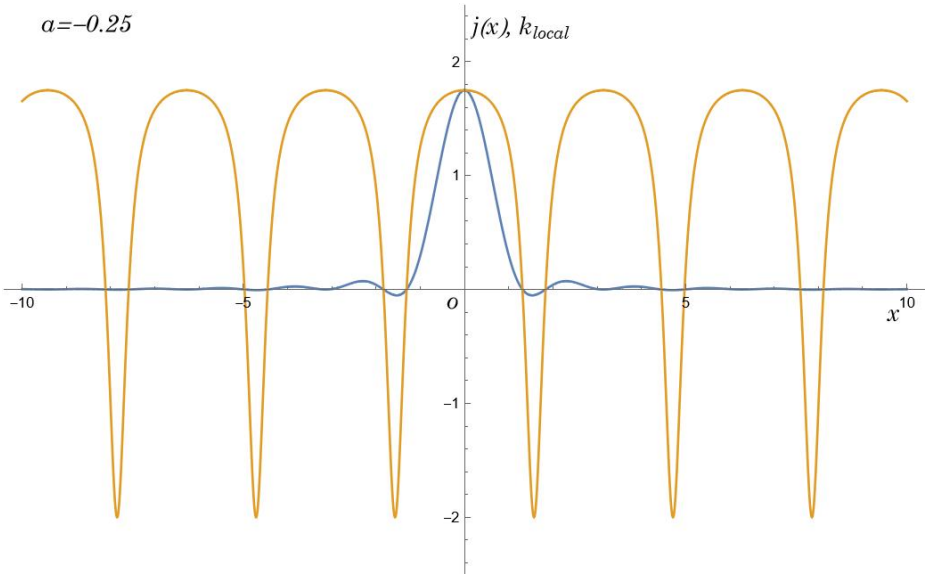

Figure 2.7: Oscillating probability flux and local momentum.
Oscillating probability flux (blue) and local momentum (yellow) for the wave function (2.36) with $a = -0.25$. One can observe that both quantities have the same sign. In particular, all negative values indicate backflow.

talks about dynamics. In order to calculate the change in probability one has to solve the corresponding time evolution and look at $\psi(x, t)$. The gain is that this definition is directly experimentally relevant. The next section will be focused on giving a concrete practical example of this type of backflow. (Possibly varify the relation using continuity equations)

CHAPTER 3

EXPERIMENTALLY ACCESSIBLE EXAMPLE

The main point of this thesis is a simple and experimentally relevant example of quantum backflow. Consider a single slit experiment with individual quanta. The probability that a particle crosses the slit can be well approximated by a flat distribution. With suitably arranged lens one observes in the focal plane the Fourier transform of the slit. This is the initial state we consider. Its momentum distribution is just flat and we will choose it purely negative (to the left). It will then be shown by a combination of analytical and numerical methods that the time evolution of this initial wave function has growing probability to find the particle to the right of carefully selected reference points.

The position-space wave function of such an initial state can be obtained from the flat distribution in momentum space:

$$\tilde{\psi}(p, t=0) = \begin{cases} 1/\sqrt{w} & \text{if } p \in [p_0 - w/2, p_0 + w/2], \\ 0 & \text{else.} \end{cases} \tag{3.1}$$

To write the wave function in position-space we calculate the inverse Fourier transform of the momentum wave function. Here instead of wave number k we use momentum p, the relation between them is $p = \hbar k$, and hence the inverse Fourier transform is modified from Eq.(2.2) to read:

$$\tilde{\psi}(p) = \frac{1}{\sqrt{2\pi\hbar}} \int_{-\infty}^{\infty} dp\, \tilde{\psi}(p)\, e^{-ipx/\hbar}. \tag{3.2}$$

One finds that the initial wave function is given by:

$$\psi(x, t=0) = \sqrt{\frac{w}{2\hbar\pi}} \mathrm{sinc}\left(\frac{wx}{2\hbar}\right) e^{ip_0 x/\hbar}. \tag{3.3}$$

3.1 Numerical Evidence of Backflow in Single Slit Experiment

Consider as the initial state the Sinc wave function with its constant momentum distribution centered at p_0, given by Eq.(3.3), where w is the width in the momentum space ($w > 0$). We always choose p_0 and w such that only negative global momentum is observed. Recall the backflow definition is given by the increased probability of observing the particle to the right of a certain reference point x_0. We therefore compute the time-evolved wave function:

$$\psi(x,t) = \frac{1}{\sqrt{2\pi\hbar w}} \int_{p_0-w/2}^{p_0+w/2} dp\, e^{-\frac{it}{\hbar}\frac{p^2}{2m}} e^{ipx/\hbar}. \tag{3.4}$$

With this at hand one computes the probability to find the particle to the right of the reference point x_0:

$$P_t(x \geq x_0) = \int_{x_0}^{\infty} |\psi(x,t)|^2 dx. \tag{3.5}$$

By following these steps one finds that the corresponding integrals are numerically expensive, but with many iterations satisfactory results are obtained. In particular, a concrete example of backflow is given in Fig. 3.1, where the probability to observe the particle to the right of point $x_0 = 2$ grows by about 0.5% starting with $p_0 = -1.5$ and $w = 3$ (unitless). In the same configuration, one could also examine the probability to observe the particle to

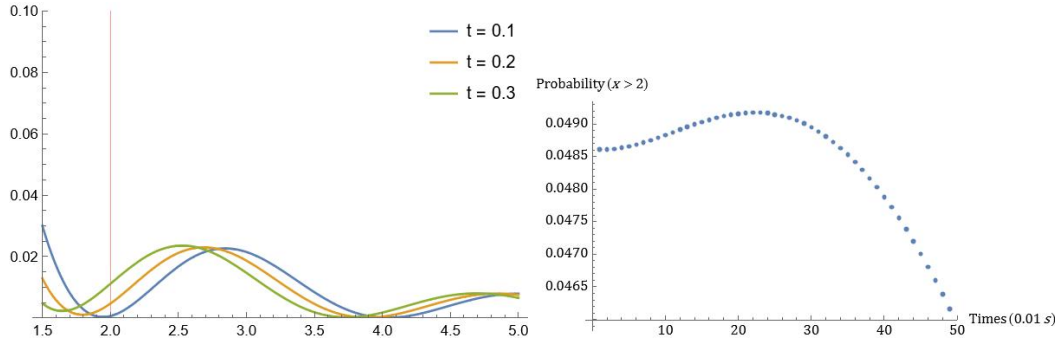

(a) Probability Distribution (b) Probability Evaluated

Figure 3.1: Evolution of probability distribution.
(a) The evolution of probability density $|\psi(x,t)|^2$ as time evolves from 0.1s to 0.3s (the three curves). The probability density broadens as the time evolves and it moves to the left. (b) The probability to find the particle to the right of point $x_0 = 2$ (see vertical line in panel (a)) as time evolves. The increase in panel (b) indicates the backflow effect.

the right of any reference point x_0 at a given time t_0. It turns out there are many other x_0

where one observes the locally increasing probability, given Fig. 3.2 for the details.

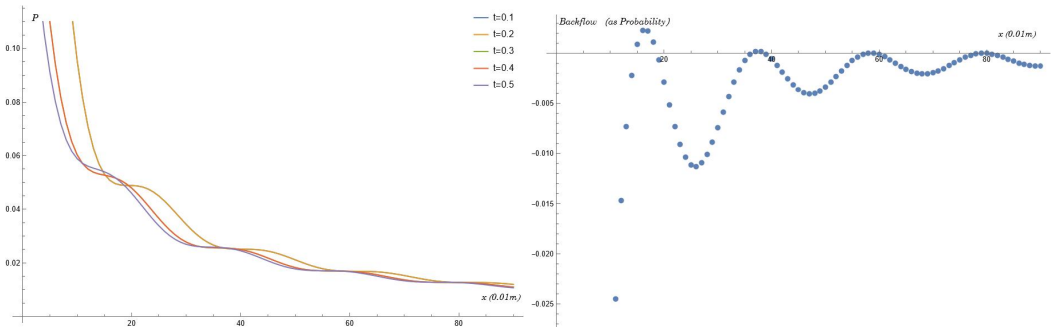

(a) Probability Distribution (b) Backflow Percentage

Figure 3.2: Spacial distribution of backflow.
(a) The evolution of probability distribution to find the particle to the right of a particular x_0, i.e. the horisontal axis shows x_0 and the vertical axis shows the result of integration in Eq. (3.5). The curves represent the time evolution from $t = 0.1$ to $t = 0.5$. (b) The backflow as measured by the difference in probabilities to observe the particle to the right of point x_0, i.e. the horisontal axis shows x_0 and the vertical axis gives the difference $P_{t_f}(x > x_0) - P_{t_i}(x > x_0)$, where we choose the final time to be $t_f = 0.5$ s and the initial time is $t_i = 0.1$ s. According to this definition backflow accurs for all positive values in the plot. This is clearly seen around point $x_0 = 1.7$, but in fact small backflow is also present around points $x_0 = 3.7$ and $x_0 = 5.5$. Note also that these results are for fixed values of initial and final time and in principle the backflow could be larger for a different choice of t_f and t_i.

In these numerical evidences, one can clearly observe the backflow even in a sinc wave packet. A reasonable conjecture could be formulated based on the numerically observed properties: the sinc wave broadens itself as time evolves, all the peaks (the main one and smaller side peaks) broaden and hence the maximum of the wave function quickly drops to keep normalisation. At the same time the purely negative momenta move the wave function to the left. The backflow occurs for delicately chosen reference points x_0 where the part of the area below the probability density curve that moved to the left is smaller than the part introuced by the broadening. This intuition is confirmed in Fig. 3.2 where panel (b) shows that backflow is occuring next to the minima of the initial wave function, which are the points most susceptible to changes due to broadening and movement.

3.2 Analytical Derivation

Numerical analysis of the previous section shows definitely that backflow happens in the considered simple system. However, the single-slit configuration is simple enough to obtain analytical results, though even in this case certain non-trivial mathematical concepts arise.

Consider the position-space wave function given by Eq. (3.4). The upper and lower limit of the integral could be simplified with the substitution $p \to p - p_0$:

$$\psi(x,t) = \frac{e^{-ip_0^2 t/2\hbar m + ip_0 x/\hbar}}{\sqrt{2\pi\hbar w}} \int_{-w/2}^{w/2} dp\, e^{-ip^2 t/2\hbar m} e^{ip(x-p_0 t/m)/\hbar}. \tag{3.6}$$

The probability density distribution in position space then reads:

$$P(x,t) = |\psi(x,t)|^2 = \frac{1}{2\pi\hbar w} \int_{-w/2}^{w/2} dp \int_{-w/2}^{w/2} dp' e^{-i(p'^2-p^2)t/2\hbar m} e^{i(p'-p)(x-p_0 t/m)/\hbar}. \tag{3.7}$$

In order to arrive at unitless quantitites (easier to optimise numerically), we implement the following change of two variables:

$$u = \frac{p+p'}{2}, \qquad v = p' - p. \tag{3.8}$$

When changing two variables the integration measure must be multipled by the Jacobian of the transformation. We therefore compute:

$$J = \begin{vmatrix} \frac{\partial p}{\partial u} & \frac{\partial p}{\partial v} \\ \frac{\partial p'}{\partial u} & \frac{\partial p'}{\partial v} \end{vmatrix} = \begin{vmatrix} 1 & -1/2 \\ 1 & 1/2 \end{vmatrix} = 1, \tag{3.9}$$

where we used the transformation rules:

$$p = u - \frac{v}{2}, \qquad p' = u + \frac{v}{2}. \tag{3.10}$$

According to this change of the variables, the integration limits in Eq. (3.7) are modified as

Fig.3.3:

$$
\begin{aligned}
P(x,t) &= \int_{-w/2}^{w/2} dp \int_{-w/2}^{w/2} dp' f(p,p') \\
&= \int_{-w/2}^{0} du \int_{-w-2u}^{w+2u} dv f(u,v) + \int_{0}^{w/2} du \int_{-w+2u}^{w-2u} dv f(u,v) \\
&= \int_{-w/2}^{w/2} du \int_{-w+2|u|}^{w-2|u|} dv f(u,v) \\
&= \frac{1}{2\pi\hbar w} \int_{-w/2}^{w/2} du \int_{-w+2|u|}^{w-2|u|} dv\, e^{iv[x-(p_0+u)t/m]/\hbar}, \qquad (3.11)
\end{aligned}
$$

The probability of finding the particle right of the reference point x_0 is accordingly given

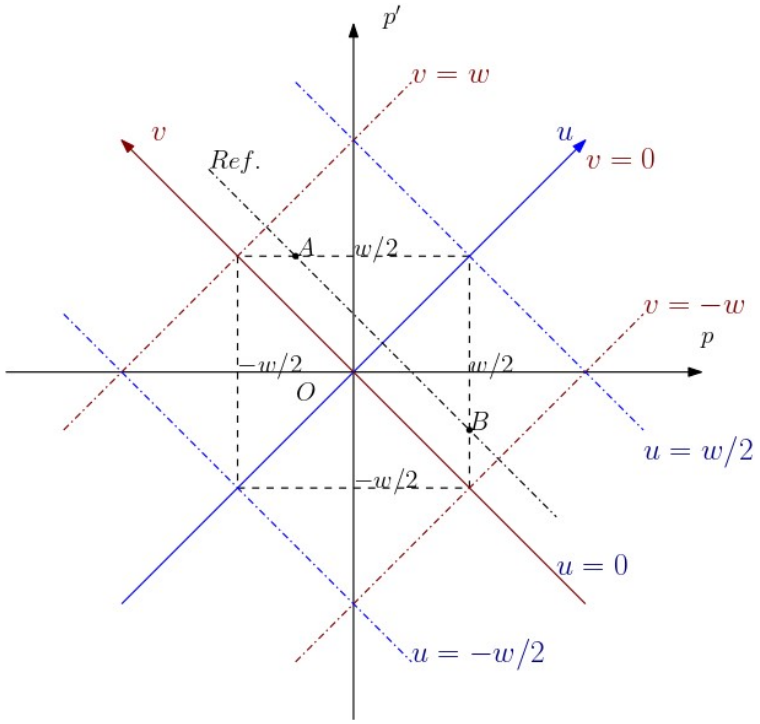

Figure 3.3: Change of upper and lower limit of the integral.
The upper and lower limit of u and v can be evaluated via their relation with p' and p. For example, at point A, $p' = u + |v|/2 = w/2$, therefore $|v| = w - 2u$; and at point B, $p = u - |v|/2 = w/2$, similarly, $|v| = -w + 2u$. Therefore, the upper and lower limit of integration over v is given. Then the integration over u is given by the upper and lower limit of value of u, i.e., $\pm w/2$.

by:

$$\begin{aligned} P_{x>x_0} &= \int_{x_0}^{\infty} dx\, P(x,t) \\ &= \frac{1}{2\pi\hbar w}\int_{-w/2}^{w/2} du \int_{-w+2|u|}^{w-2|u|} dv e^{-iv(p_0+u)t/m\hbar}\int_{x_0}^{\infty} dx\, e^{ivx/\hbar} \\ &= \frac{1}{2\pi\hbar w}\int_{-w/2}^{w/2} du \int_{-w+2|u|}^{w-2|u|} dv\, e^{iv[x_0-(p_0+u)t/m]/\hbar}\int_{0}^{\infty} dx\, e^{ivx/\hbar}, \end{aligned} \tag{3.12}$$

where in the last equation we subsituted $x \to x - x_0$. The integration over x can be evaluated using the well-known Sokhotski-Plemelj formula [Julve et al., 2016]:

$$\int_0^{\infty} dx\, e^{ivx/\hbar} = i\,\mathrm{P.V.}\,\frac{\hbar}{v} + \pi\delta(v/\hbar) = i\hbar\,\mathrm{P.V.}\,\frac{1}{v} + \pi\hbar\delta(v) \tag{3.13}$$

where the $\mathrm{P.V.}$ stands for the Cauchy principal value and we used the scaling property of Dirac delta. The overall Eq. (3.12) is then reformed as:

$$P_{x>x_0} = \frac{1}{2\pi\hbar w}\int_{-w/2}^{w/2} du \int_{-w+2|u|}^{w-2|u|} dv\, e^{iv[x_0-(p_0+u)t/m]/\hbar}[\pi\hbar\delta(v)] + \tag{3.14}$$

$$\frac{i}{2\pi w}\int_{-w/2}^{w/2} du \int_{-w+2|u|}^{w-2|u|} dv\, e^{iv[x_0-(p_0+u)t/m]/\hbar}\left[\mathrm{P.V.}\,\frac{1}{v}\right] \tag{3.15}$$

The first part can be directly evaluated:

$$\frac{1}{2\pi\hbar w}\int_{-w/2}^{w/2} du \int_{-w+2|u|}^{w-2|u|} dv\, e^{iv[x_0-(p_0+u)t/m]/\hbar}[\pi\hbar\delta(v)] = \frac{1}{2}. \qquad (w>0) \tag{3.16}$$

The second part can be simplified using the definition of the Cauchy principal value. It states that the integration over v can be computed by taking the integration limits approach-

ing the singular point $v = 0$ as follows:

$$\begin{aligned}
&\lim_{\epsilon\to+0}\left(\int_{-w+2|u|}^{-\epsilon}\frac{dv}{v}e^{iv[x_0-(p_0+u)t/m]/\hbar}+\int_{\epsilon}^{w-2|u|}\frac{dv}{v}e^{iv[x_0-(p_0+u)t/m]/\hbar}\right)\\
=&\lim_{\epsilon\to+0}\left(-\int_{\epsilon}^{w-2|u|}\frac{dv}{v}e^{-iv[x_0-(p_0+u)t/m]/\hbar}+\int_{\epsilon}^{w-2|u|}\frac{dv}{v}e^{iv[x_0-(p_0+u)t/m]/\hbar}\right)\\
=&\lim_{\epsilon\to+0}\int_{\epsilon}^{w-2|u|}\frac{dv}{v}(e^{iv[x_0-(p_0+u)t/m]/\hbar}-e^{-iv[x_0-(p_0+u)t/m]/\hbar})\\
=&\int_0^{w-2|u|}\frac{dv}{v}\,2i\sin\left(\frac{x_0-(p_0+u)t/m}{\hbar}v\right)\\
=&\;2iC\int_0^{[x_0-(p_0+u)t/m](w-2|u|)/\hbar}\frac{dv}{v}\sin v. \qquad (3.17)
\end{aligned}$$

The last integral is a special case of general sine integral function $\mathrm{Si}(z)$:

$$\mathrm{Si}(z)=\int_0^z\frac{dv}{v}\sin v, \qquad (3.18)$$

which is widely numerically implemented, and the overall probability of finding the particle right of reference point x_0 reads:

$$P_{x>x_0}=\frac{1}{2}-\frac{1}{\pi w}\int_{-w/2}^{w/2}du\,\mathrm{Si}\left(\frac{x_0-(p_0+u)t/m}{\hbar}(w-2|u|)\right). \qquad (3.19)$$

Alternatively, the same result is obtained perhaps more directly with the help of contour integral [Brown and Churchill, 2009]. Consider integration over x in Eq. (3.12):

$$\int_0^\infty dx\,e^{ivx/\hbar}=\lim_{\epsilon\to+0}\int_0^\infty dx\,e^{ivx/\hbar-\epsilon x}=\lim_{\epsilon\to+0}\frac{1}{iv/\hbar-\epsilon}e^{(iv/\hbar-\epsilon)x}\Big|_0^\infty=\lim_{\epsilon\to+0}\frac{-i\hbar}{v+i\hbar\epsilon} \qquad (3.20)$$

where the steps are justified as follows. Since $e^{ivx/\hbar}$ is an oscillating function of x, its integral is undefined at infinity. In the first step we multiply this function by exponentially decaying factor $e^{-\epsilon x}$ so that the total integrand is now equal to zero at infinity. The idea is to evaluate such obtained integral and then take the limit $\epsilon\to 0$. Now we move to integration over v:

$$(-i\hbar)\lim_{\epsilon\to+0}\int_{-w+2|u|}^{w-2|u|}dv\,e^{iv[x_0-(p_0+u)t/m]/\hbar}\frac{1}{v+i\hbar\epsilon}. \qquad (3.21)$$

The limit over ϵ is kept outside the integral, so that it is clear that the integrand function has a complex pole at $v = -i\hbar\epsilon$. The residue theorem states that:

$$\oint_C f(z)dz = 2\pi i \,\mathrm{Res}(f), \tag{3.22}$$

where the integral is over positively oriented curve C (such that when moving on it the interior is on the left) that winds around the pole, and $\mathrm{Res}(f, p)$ stands for the residue, computed as follows:

$$\mathrm{Res}(f, p) = \lim_{z\to p}(z - p)f(z), \tag{3.23}$$

where p stands for the pole. In our case, $f(z) = e^{izC/\hbar}\frac{1}{v+i\hbar\epsilon}$, where for brevity we introduced constant C. Hence the residue is equal to:

$$\mathrm{Res}(f) = e^{\epsilon C} \to 1 \tag{3.24}$$

where the limit is for $\epsilon \to 0$. Since the pole of the function is negative and lies along the imaginary axis in the complex plane, see Fig. 3.4, and we aim at determining the integral from $a = w - 2|u|$ to $-a = -w + 2|u|$, we choose the integration curve as a line from a to $-a$ along the real axis and a semi-circle of radius a winding the pole, which is a positive oriented curve. Here, for further simplicity, we replace $[x_0 - (p_0 + u)t/m]/\hbar$ with C and we denoted the original integral over v as "ANS":

$$\mathrm{ANS} = (-i\hbar)\lim_{\epsilon\to+0}\int_{-a}^{a}\frac{dv}{v + i\hbar\epsilon}e^{ivC/\hbar}, \tag{3.25}$$

and thus:

$$-\mathrm{ANS} = (-i\hbar)\lim_{\epsilon\to+0}\int_{a}^{-a}\frac{dv}{v + i\hbar\epsilon}e^{ivC/\hbar}, \tag{3.26}$$

Finally, applying the residue theorem with $v = ae^{i\theta}$,$dv = iae^{i\theta}d\theta$ and approach ϵ to 0, this gives:

$$2\pi i\mathrm{Res} =\to 2\pi i = -\mathrm{ANS} + \int_{\pi}^{2\pi} d\theta\, ie^{aCe^{i\theta}/\hbar}, \tag{3.27}$$

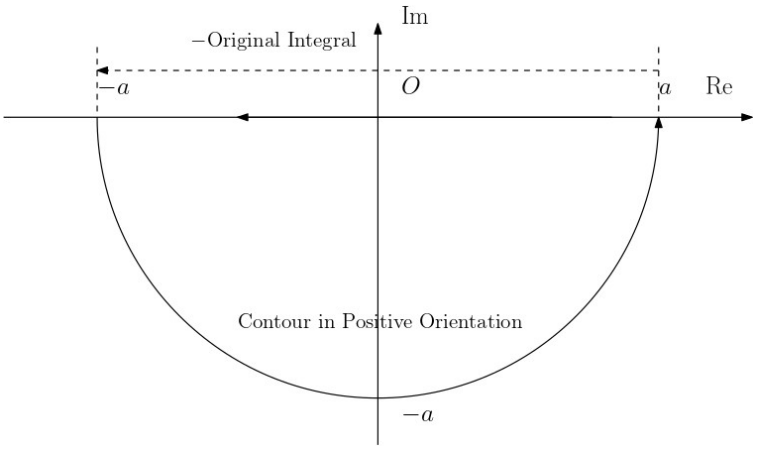

Figure 3.4: Inversely oriented curve of the integral.

thus,

$$\begin{aligned} \text{ANS} &= \int_{\pi}^{2\pi} d\theta\, ie^{aCe^{i\theta}/\hbar} - 2\pi i \\ &= \pi i + 2i\,\text{Si}(aC/\hbar) - 2\pi i \\ &= 2i\,\text{Si}(aC/\hbar) - \pi i. \end{aligned} \tag{3.28}$$

put everything back while substitute back the value of a and C:

$$\frac{1}{2\pi\hbar w}\int_{-w/2}^{w/2} du\; -(i\hbar)\pi i - \frac{1}{\pi w}\int_{-w/2}^{w/2} du\,\text{Si}\left(\frac{x_0-(p_0+u)t/m}{\hbar}(w-2|u|)\right), \tag{3.29}$$

the former part of integration returns $1/2$, and therefore, the final result remains the same:

$$P_{x>x_0} = \frac{1}{2} - \frac{1}{\pi w}\int_{-w/2}^{w/2} du\,\text{Si}\left(\frac{x_0-(p_0+u)t/m}{\hbar}(w-2|u|)\right). \tag{3.30}$$

And thus prove the analytical solution.

The obtained solution can be used to provide high resolution graph of the probability $P_{x>x_0}$, for an example see Fig. 3.5.

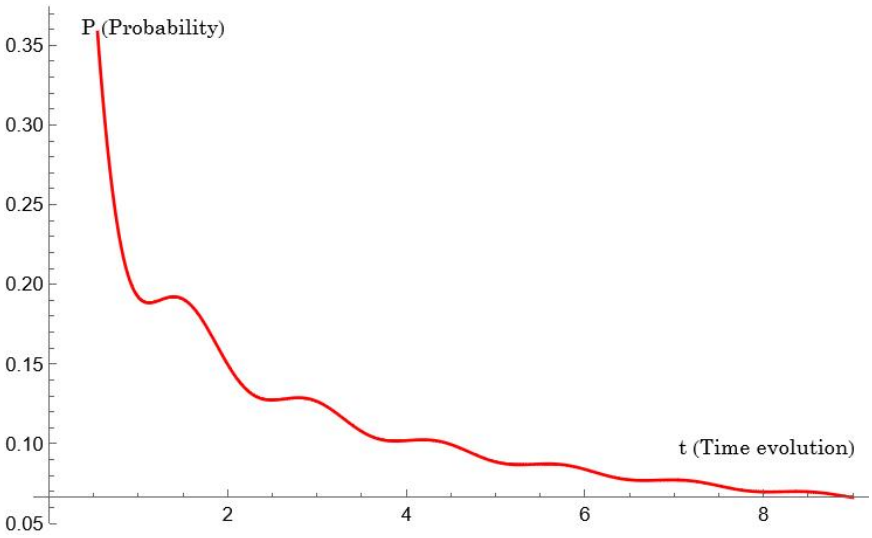

Figure 3.5: Analytical approach to backflow.
Probability to find the particle to the right of point $x_0 = 2$ using analytical expression (3.19). Here $p_0 = -1.5$ and $w = 3$ (unitless). Each increase in the plot represents the presence of backflow.

CHAPTER 4

DISCUSSION ON THE EXAMPLE

We would like to propose an intuitive understanding about the origin of backflow in the single-slit experiment. On one hand, one has purely negative global momentum, which shifts the whole wave function in one direction, in this case to the left. Yet, in quantum mechanics all freely evolving wave functions spread in time. In may therefore happen that the probability which “escaped” from the region to the right of some reference point x_0 is actually smaller than the probability that was “added” by the spread of the free evolution. An observation that supports this intuition is that backflow happens around the points where the initial probability density has minima.

Furthermore, such understanding could be illustrated by the graph provided by our analytical solution:

As observed, dynamical backflow happens exactly at those times where the time evolution makes the probability of the particle right of the reference point x_0, while always have lagged behind the local minima of the probability distribution at time $t = 0$. This could be explained by the all negative global momentum p, which leads the wave as well as the probability distribution leftward as time evolves. This would also result in the local minima of the probability distribution moving left, which effectively cause the "lag" between backflow and local minima ($t = 0$).

Also, recall that such wave will broaden itself while time evolving, and would effectively push the local minimums away from each other. This would result in the "lag" between each local minima and backflow "hotspots" from left to right, appearing progressively larger. This effect could also be observed in the panel (b) of Fig. 4.1, where the "lag" appears to be larger and larger for each backflow "hotspots" form left to right.

The thesis was focused on providing a simple example and due to time constraints we were not able to optimise the effect over experimentally relevant sets of parameters. The figure of

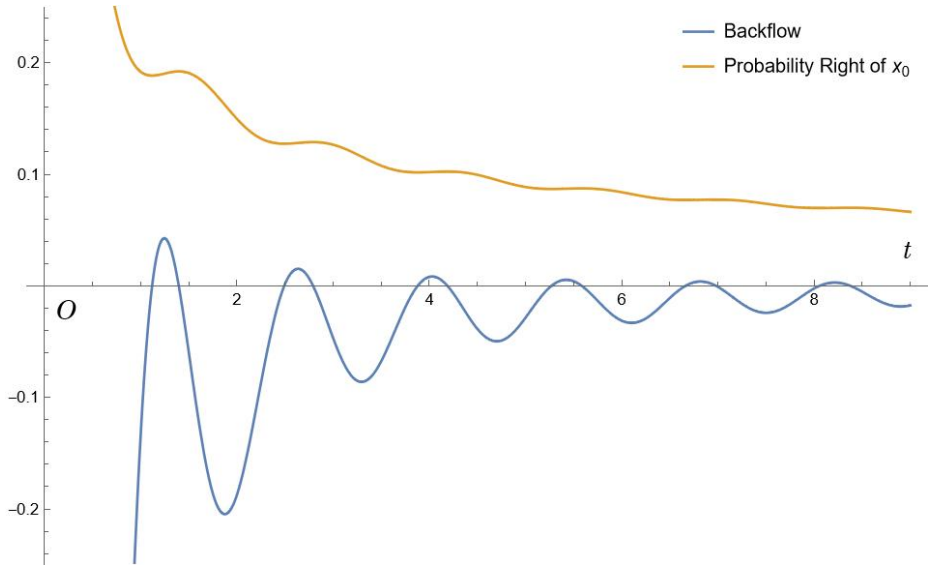

(a) Backflow and Probability distribution

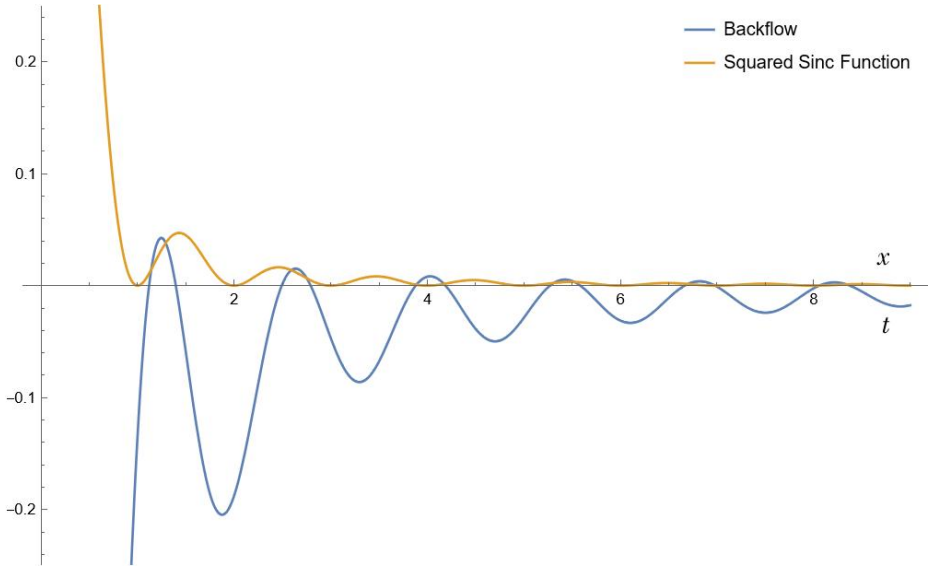

(b) Backflow and Squared original wave function

Figure 4.1: Backflow analysis on spacial distribution and time-evolution.
Panel (a) provides the backflow plotting against the probability of finding the particle right of the reference point x_0 in a time evolving from 0.1 to 0.9 (dimensionless). Panel (b) provides the backflow plotting against the squared original wave function (which gives the probability distribution at $t = 0$). In both panels, backflow happens when the backflow curve is above 0.

merit that one would like to maximise is the difference between $P_t(x \geq x_0) - P_{t_0}(x \geq x_0)$ where t_0 denotes the time where the probability has local (in time) minimum.

CHAPTER 5

CONCLUSION

The thesis provides review of concepts used to define the quantum backflow effect. These include: local momentum (local wave number), superoscillation (and suboscillation), probability current and probability to locate the particle in a particular region in space. The backflow occurs when the local momentum is opposite to global momentum and all global momentum spectrum has one sign. It can also be defined as probability current being opposite locally to global momentum. We showed that both definitions are equivalent. In the third approach the backflow occurs when the probability to find the particle say to the right of reference point grows despite only negative global momentum. We provided an experimentally viable example of this sort: a flat distribution of momentum, which gives us a sinc function in position representation turns out to be backflowing. The predicted amount of backflow is 0.5%, which is challenging and perhaps could be improved in further research.

REFERENCES

[Aharonov et al., 2011] Aharonov, Y., Colombo, F., Sabadini, I., Struppa, D., and Tollaksen, J. (2011). Some mathematical properties of superoscillations. *Journal of Physics A: Mathematical and Theoretical*, 44(36):365304.

[Allcock, 1969] Allcock, G. R. (1969). The time of arrival in quantum mechanics i. formal considerations. *Annals of physics*, 53(2):253–285.

[Allen and Padgett, 2011] Allen, L. and Padgett, M. (2011). The orbital angular momentum of light: An introduction. *Twisted Photons: Applications of Light with Orbital Angular Momentum*, pages 1–12.

[Berry, 2013a] Berry, M. (2013a). Five momenta. *European Journal of Physics*, 34(6):1337.

[Berry, 2013b] Berry, M. (2013b). A note on superoscillations associated with bessel beams. *Journal of Optics*, 15(4):044006.

[Berry and Popescu, 2006] Berry, M. and Popescu, S. (2006). Evolution of quantum superoscillations and optical superresolution without evanescent waves. *Journal of Physics A: Mathematical and General*, 39(22):6965.

[Bracken and Melloy, 1994] Bracken, A. and Melloy, G. (1994). Probability backflow and a new dimensionless quantum number. *Journal of Physics A: Mathematical and General*, 27(6):2197.

[Brown and Churchill, 2009] Brown, J. W. and Churchill, R. V. (2009). *Complex variables and applications*. McGraw-Hill,.

[Chen et al., 2019] Chen, G., Wen, Z.-Q., and Qiu, C.-W. (2019). Superoscillation: from physics to optical applications. *Light: Science & Applications*, 8(1):56.

[Daniel et al., 2022] Daniel, A., Ghosh, B., Gorzkowski, B., and Lapkiewicz, R. (2022). Demonstrating backflow in classical two beams' interference. *New Journal of Physics*, 24(12):123011.

[Dennis et al., 2008] Dennis, M. R., Hamilton, A. C., and Courtial, J. (2008). Superoscillation in speckle patterns. *Optics letters*, 33(24):2976–2978.

[Eliezer and Bahabad, 2017] Eliezer, Y. and Bahabad, A. (2017). Super defocusing of light by optical sub-oscillations. *Optica*, 4(4):440–446.

[Eliezer et al., 2020] Eliezer, Y., Zacharias, T., and Bahabad, A. (2020). Observation of optical backflow. *Optica*, 7(1):72–76.

[Ghosh et al., 2023] Ghosh, B., Daniel, A., Gorzkowski, B., and Lapkiewicz, R. (2023). Azimuthal backflow in light carrying orbital angular momentum.

[Holland, 1995] Holland, P. R. (1995). *The quantum theory of motion: an account of the de Broglie-Bohm causal interpretation of quantum mechanics*. Cambridge university press.

[Julve et al., 2016] Julve, J., Cepedello, R., and de Urries, F. (2016). The complex dirac delta, plemelj formula, and integral representations. *arXiv preprint arXiv:1603.05530*.

[Kijowski, 1974] Kijowski, J. (1974). On the time operator in quantum mechanics and the heisenberg uncertainty relation for energy and time. *Reports on Mathematical Physics*, 6(3):361–386.

[Madelung, 1927] Madelung, E. (1927). Quantetheorie in hydrodynamischer form, z. *Physik*, 40:322.

[Penz et al., 2005] Penz, M., Grübl, G., Kreidl, S., and Wagner, P. (2005). A new approach to quantum backflow. *Journal of Physics A: Mathematical and General*, 39(2):423–433.

[Rogers and Zheludev, 2013] Rogers, E. T. and Zheludev, N. I. (2013). Optical super-oscillations: sub-wavelength light focusing and super-resolution imaging. *Journal of Optics*, 15(9):094008.

[Wilson and McCreary, 1995] Wilson, R. G. and McCreary, S. M. (1995). Fourier series and optical transform techniques in contemporary optics: an introduction. *(No Title)*.

[Yuan et al., 2017] Yuan, G. H., Rogers, E. T., and Zheludev, N. I. (2017). Achromatic super-oscillatory lenses with sub-wavelength focusing. *Light: Science & Applications*, 6(9):e17036–e17036.

[Zheludev and Yuan, 2022] Zheludev, N. I. and Yuan, G. (2022). Optical superoscillation technologies beyond the diffraction limit. *Nature Reviews Physics*, 4(1):16–32.